MULTISCALE DEFORMABLE REGISTRATION OF NOISY MEDICAL IMAGES

Dana Paquin

Department of Mathematics, Kenyon College
Gambier, OH 43022-9623

Doron Levy

Department of Mathematics
Center for Scientific Computations and Mathematical Modeling (CSCAMM)
University of Maryland
College Park, MD 20742-3281

Lei Xing

Department of Radiation Oncology, Stanford University
Stanford, CA 94305-5947

Abstract. Multiscale image registration techniques are presented for the registration of medical images using deformable registration models. The techniques are particularly effective for registration problems in which one or both of the images to be registered contains significant levels of noise. A brief overview of existing deformable registration techniques is presented, and experiments using B-spline free-form deformation registration models demonstrate that ordinary deformable registration techniques fail to produce accurate results in the presence of significant levels of noise. The hierarchical multiscale image decomposition described in E. Tadmor, S. Nezzar, and L. Vese's, "A multiscale image representation using hierarchical (BV, L^2) decompositions" (*Multiscale Modeling and Simulations*, 2 (2004): 4, pp. 554–579) is reviewed, and multiscale image registration algorithms are developed based on the multiscale decomposition. Accurate registration of noisy images is achieved by obtaining a hierarchical multiscale decomposition of the images and iteratively registering the resulting components. This approach enables a successful registration of images that contain noise levels well beyond the level at which ordinary deformable registration fails. Numerous image registration experiments demonstrate the accuracy and efficiency of the multiscale registration techniques.

1. **Introduction.** Image registration is the process of determining the optimal spatial transformation that maps one image to another. Image registration is necessary, for example, when images of the same object are taken at different times, from different imaging devices, or from different perspectives. The two images to be registered, called the fixed and moving images, are the input to the registration algorithm, and the output is the optimal transformation that maps the moving image to the fixed image. Ideally, the transformed moving image should be identical

to the fixed image after registration. Applications of image registration include radiation therapy, image-guided surgery, functional MRI analysis, and tumor detection, as well as many nonmedical applications, such as computer vision, pattern recognition, and remotely sensed data processing (see [4], [11], and the references therein).

Image registration models are classified into two main categories according to the transformation type: rigid and deformable. Rigid image registration models assume that the transformation that maps the moving image to the fixed image consists only of translations and rotations. While such models are sufficient for many applications, it is clear that many registration problems, particularly in medical imaging, are nonrigid. For example, respiratory motion causes nonrigid, or deformable, distortion of the lungs, which in turn results in a distortion of other organs. As another example, in neurosurgery brain tumors are typically identified and diagnosed using magnetic resonance images (MRI), but stereotaxy technology (the use of surgical instruments to reach specified points) generally uses computed tomography (CT) images. Registration of these modalities allows the transfer of coordinates of tumors from the MRI images to the CT images. However, if the tumor changes its shape, size, or position, the surrounding brain matter will deform in a nonrigid way. Additionally, during surgery the spatial coordinates of brain structures deform significantly due to leakage of cerebrospinal fluid, administration of anesthetic agents, hemmorhage, and retraction and resection of tissue. Image-guided neurosurgery procedures thus require registration of pre- and intra-operative images of the brain. See [15] and [19] for a discussion of the use of deformable registration in neurosurgery.

This paper is an extension of [13], in which we presented a multiscale approach to rigid registration of medical images. In this paper, we apply the multiscale registration algorithm of [13] to deformable registration problems. While our method can be used in conjunction with any registration model, we choose to focus on B-spline free form deformation (FFD) models.

The structure of this paper is as follows. In Section 2, we provide a brief overview of the image registration problem and discuss deformable registration techniques. In Section 3, we present the problem of deformable image registration in the presence of noise, and illustrate the failure of standard FFD techniques when one or both of the images to be registered contains significant levels of noise. In Section 4, we review the hierarchical multiscale image decomposition of [18], and we present two multiscale image registration algorithms based on the decomposition. In Section 5, we demonstrate the accuracy and efficiency of our multiscale registration techniques with several image registration experiments. Concluding remarks are given in Section 6.

2. The registration problem.

Given a *fixed* and a *moving* image, the registration problem is the process of finding an *optimal transformation* that brings the moving image into spatial alignment with the fixed image. While this problem is easy to state, it is difficult to solve. The main source of difficulty is that the problem is ill-posed, which means, for example, that the problem may not have a unique solution. Additionally, the notion of optimality may vary for each application: for example, some applications may require consideration only of rigid transformations, while other applications require nonrigid transformations, while still other applications may require structural correspondence of anatomical structures. Finally,

computation time and data storage constraints place limitations on the complexity of models that can be used for describing the problem. For a detailed overview of the image registration problem and various image registration techniques, see [12].

To formulate the registration problem mathematically, a two-dimensional gray-scale image f is a mapping which assigns to every point $x \in \Omega \subset \mathbb{R}^2$ a gray value $f(x)$ (called the intensity value of the image at the point x). We will consider images as elements of the space $L^2(\mathbb{R}^2)$. Any registration algorithm has three main components:

1. the *transformation model*, which specifies the way in which the moving image can be transformed to correspond to the fixed image;
2. the *distance measure*, or metric, used to compare the fixed and moving images;
3. the *optimization process*, that varies the parameters of the transformation model in such a way that the transformation produced by the registration process is optimal.

Given a distance measure $D : (L^2(\mathbb{R}^2))^2 \to \mathbb{R}$ and two images $f(x), m(x) \in L^2(\mathbb{R}^2)$, the solution ϕ of the registration problem is given by the following minimization problem:

$$\phi = \underset{\psi:\mathbb{R}^2\to\mathbb{R}^2}{\operatorname{argmin}} D(f(x), m(\psi(x))), \tag{1}$$

where ψ is in the specified space of transformation models. Examples of commonly used distance measures are mean squares, normalized correlation, and mutual information. Examples of typical transformation models are rigid, affine, polynomial, and spline transformations [12]. To minimize $D(f, m(\psi))$, we must choose an optimizer which controls the minimization. The most commonly used optimization techniques in image registration are gradient descent and regular step-gradient descent methods. The implementation of the registration algorithm works in the following way: at each iteration, the distance D between the two images is computed. The specified transformation is then applied to the moving image, and the distance between the images is recomputed. In theory, this process continues until the distance is minimized (or maximized in certain cases), though in practice a stopping criterion is applied.

Historically, image registration problems have been classified as either *rigid* or *nonrigid*. In rigid registration problems, the moving image is assumed to differ from the fixed image by translation and/or rotation. Thus rigid registration techniques involve the determination of only a small number of parameters. In nonrigid, or *deformable* rigid registration problems, the correspondence between the two images involves a localized stretching of the images. As most of the organs in the human body are not confined to rigid motion, much of the current work in medical image registration is focused on the deformable case. Although deformable image registration clearly allows for more flexibility in the types of images and applications in which it can be used, deformable registration techniques require significantly more computation time than rigid registration techniques, and involve the determination of a very large number of parameters. In this paper, we shall focus on the problem of deformable registration in the presence of noise. This is an extension of our work on rigid registration in the presence of noise, [13].

2.1. **Deformable registration techniques.** Spline-based FFD transformation models are among the most common and important transformation models used

in nonrigid registration problems [6] and [17]. Spline-based registration algorithms use *control* points in the fixed image and a spline function to define transformations away from these points. The two main spline models used in registration are *thin-plate splines* and *B-splines*. Thin-plate splines have the property that each control point has a global influence on the transformation. That is, if the position of one control point is perturbed, then all other points in the image are perturbed as well. This can be a disadvantage because it limits the ability of the transformation model to model localized deformations. In addition, the computation time required for a thin-plate spline-based registration algorithm increases significantly as the number of control points increases. See [3] for an overview of thin-plate splines.

In contrast, B-splines are only defined in the neighborhood of each control point. Thus perturbing the position of one control point affects the transformation only in a neighborhood of that point. As a result, B-spline-based registration techniques are more computationally efficient than thin-plate splines, especially for a large number of control points. See [9] and [10] for a detailed description of FFD transformation models. In this paper, we shall use deformable registration algorithms based on B-spline FFD models. To define the spline-based deformation model, let $\Omega = \{(x, y) \mid 0 \leq x \leq X,\ 0 \leq y \leq Y\}$ denote the domain of the image volume. Let α denote a $n_x \times n_y$ mesh of control points $\alpha_{i,j}$ with uniform spacing δ. Then the B-spline deformation model can be written as the 2-D tensor product of 1-D cubic B-splines:

$$\phi(x, y) = \sum_{l=0}^{3} \sum_{m=0}^{3} B_l(u) B_m(v) \alpha_{i+l, j+m}, \tag{2}$$

where $i = \lfloor x/n_x \rfloor - 1$, $j = \lfloor y/n_y \rfloor - 1$, and B_l represents the l-th basis of the B-spline:

$$\begin{aligned}
B_0(u) &= \frac{1}{6}(1-u)^3 \ , \\
B_1(u) &= \frac{1}{6}(3u^3 - 6u^2 + 4) \ , \\
B_2(u) &= \frac{1}{6}(-3u^3 + 3u^2 + 3u + 1) \ , \\
B_3(u) &= \frac{1}{6}u^3 \ ,
\end{aligned}$$

$0 \leq u \leq 1$. Changing the control point $\alpha_{i,j}$ affects the transformation only in a local neighborhood of $\alpha_{i,j}$. The control points α act as parameters of the B-spline deformation model, and the degree of nonrigid deformation that can be modeled depends on the resolution of the mesh of control points α. A large spacing of control points allows modeling of global nonrigid deformation, while a small spacing of control points allows modeling of local nonrigid deformations. Additionally, the number of control points determines the number of degrees of freedom of the transformation model, and hence, the computational complexity. For example, a B-spline deformation model defined by a 10×10 grid of control points yields a transformation with $2 \times 10 \times 10 = 200$ degrees of freedom. Thus there is a tradeoff between the model flexibility and its computational complexity.

We note in passing that there are additional deformable registration techniques such as elastic models [2], viscous fluid models [5], and finite element models [7].

EXAMPLE.Registration of a deformed image.

Consider the midsagittal brain slice I and the deformed image S, shown in Figure 1. The midsagittal brain slice I is taken from the Insight Segmentation and Registration Toolkit (ITK) data repository [8]. The deformed image S is obtained by applying a known B-spline deformation to the original image I. Since the deformation transformation that maps the deformed image S to the original image I and corresponding deformation field are known, we can effectively evaluate the accuracy of various deformable registration methods by comparing the output deformation fields with the known deformation field. For all registration simulations presented in this paper, we use a B-spline FFD registration technique with a mean squares image metric and a conjugate gradient descent algorithm. However, the multiscale registration algorithms developed in this paper are independent of the particular registration technique used to register the images.

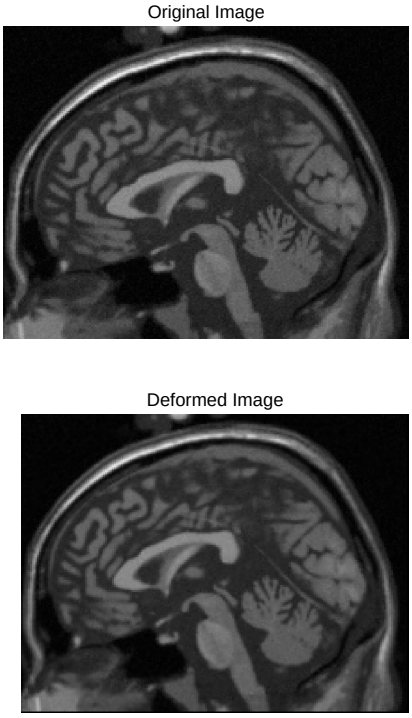

FIGURE 1. The midsagittal brain slice I (shown on the left) and the deformed image S (shown on the right).

Using an FFD registration model, the image S is successfully registered with the image I.

In Figure 2, we compare the result of the registration process, namely the image obtained upon applying the optimal deformable transformation determined by the algorithm to the deformed image, with the original image I. Ideally, both figures should be identical. Indeed, the images in Figure 2 demonstrate that the deformable

registration algorithm recovers the deformation transformation. To quantitatively evaluate the accuracy of the registration algorithm, we compare the *correlation coefficients* between the images before and after registration. The correlation coefficient $\rho(A, B)$ between two images A and B is given by:

$$\rho(A,B) = \frac{\sum_m \sum_n (A_{mn} - \bar{A})(B_{mn} - \bar{B})}{\sqrt{\sum_m \sum_n (A_{mn} - \bar{A})^2 (B_{mn} - \bar{B})^2}},$$

where A and B are $m \times n$ two-dimensional images and $\bar{A}$ and $\bar{B}$ represent the mean value of the elements of A and B, respectively. A correlation coefficient of zero indicates a low degree of matching between the images, and a correlation coefficient of 1 indicates exact similarity between the images. Correlation coefficients are a commonly used representation of similarity between images for the evaluation of deformable registration techniques [14]. Before registration, the correlation coefficient between the original and deformed images is 0.74. After registration, the correlation coefficient between the transformed moving and fixed images is 0.96.

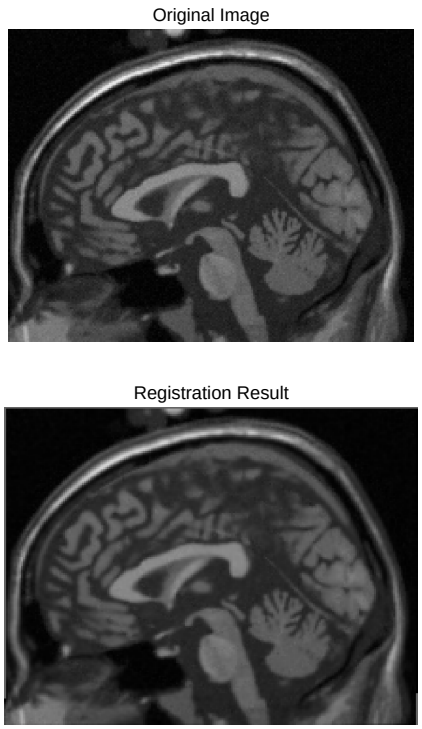

FIGURE 2. The result (shown on the right) upon registering the deformed image S with the original image I (shown on the left).

In Figure 3, we display the exact deformation field corresponding to the deformation transformation between the images I and S (on the left) and the deformation field determined by the deformable registration algorithm, and note that visually the two deformation fields are almost identical. The deformation field is

a two-dimensional vector field that represents graphically the magnitude of the deformation at each pixel in the image.

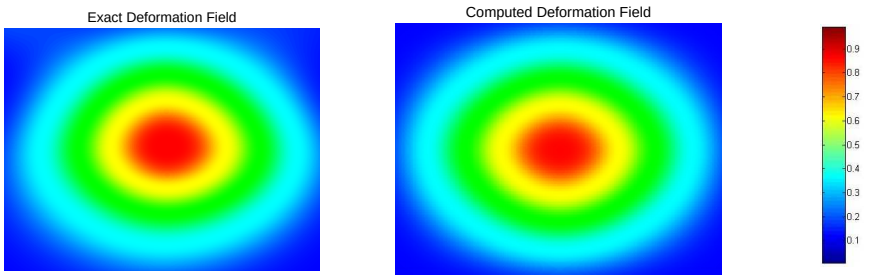

FIGURE 3. The exact deformation field corresponding to the deformation transformation between I and S (shown on the left) and the deformation field produced by the registration algorithm upon registering the deformed image S with the original image I (shown on the right).

3. **Deformation registration in the presence of noise.** In this section, we study the effect of noise on deformable registration. Again, we will consider the brain midsagittal slice I and the deformed image S from Figure 1. Initially, we will consider the registration problem in which only one of the two images (here, the moving image) is noisy. In imaging, the term *noise* refers to random fluctuations in intensity values that occur during image capture, transmission, or processing, and that may distort the information given by the image. Image noise is not part of the ideal signal and may be caused by a wide range of sources, such as detector sensitivity, environmental radiation, transmission errors, discretization effects, etc. In this paper, we will study the problem of image registration in the presence of high levels of speckle noise (though we have conducted experiments demonstrating that we obtain similar results for other types of noise). See, for example, our results for rigid registration [13].

Speckle noise, or multiplicative noise, is a type of noise that occurs commonly in medical imaging. In particular, speckle noise is often found in ultrasound images [1]. It is defined by the following model. We let $s(x)$ denote the actual image, and $f(x)$ the observed image. Then

$$f(x) = s(x) + \eta(0, \delta) \cdot s(x), \tag{3}$$

where $\eta(0, \delta)$ is uniformly distributed random noise of mean 0 and variance δ. We add speckle noise of increasing variance to the image S, as illustrated in Figure 4. For a given noise variance δ, we denote the noisy image S_δ.

In Figure 5, we illustrate the deformation fields produced by the standard FFD registration algorithm upon registering the noisy deformed images S_δ with the original image I. Recall that the actual deformation is shown in Figure 3.

A visual comparison of the deformation fields presented in Figure 5 with the exact deformation field in Figure 3 indicates that the deformation registration technique fails to produce physically meaningful results for noise variance δ greater than 0.2. To quantitatively evaluate the accuracy of the deformable registration algorithm for

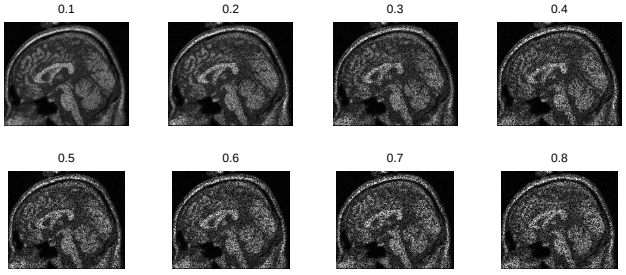

FIGURE 4. The noisy images S_δ, for increasing values of δ.

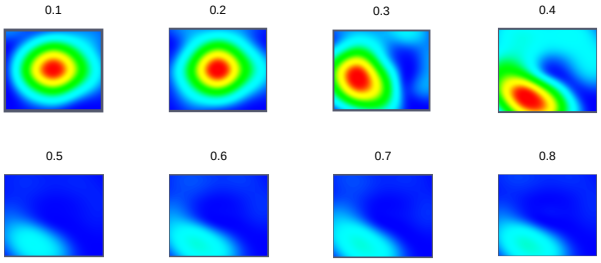

FIGURE 5. The deformation fields produced by the standard FFD registration algorithm upon registering the noisy deformed images S_δ with the original image I, for increasing values of δ.

TABLE 1. The correlation coefficient ρ between the transformed moving and fixed images after standard FFD registration for each speckle noise variance δ.

δ	0	0.1	0.2	0.3	0.4
ρ	0.96	0.90	0.85	0.75	0.69
δ	0.5	0.6	0.7	0.8	0.9
ρ	0.65	0.62	0.61	0.60	0.60

registration of the noisy images, we compute the correlation coefficients between the transformed moving and fixed images after registration for each speckle noise variance δ. In Table 1, we present the correlation coefficients ρ for each noise variance δ. For reference, we also include in the first line of Table 1 the correlation coefficients between the images after registration when the deformed image contains no noise. Recall that the maximum possible correlation coefficient is 1 and the minimum possible correlation coefficient is 0.

The results presented in Figure 5 and Table 1 indicate that ordinary deformable registration techniques fail to produce an accurate registration result when one of the images to be registered contains significant levels of noise. As expected, the level of failure increases as the speckle noise variance δ increases. For variances greater than or equal to 0.2 the algorithm fails to produce any meaningful results.

4. **Multiscale registration algorithms.**

4.1. **The multiscale decomposition.** The multiscale registration techniques to be discussed in this paper are based on the multiscale image representation using the hierarchical (BV, L^2) decompositions of [18]. This multiscale decomposition will provide a hierarchical expansion of an image that separates the essential features of the image (such as large shapes and edges) from the fine scales of the image (such as details and noise). The decomposition is hierarchical in the sense that it will produce a series of expansions of the image that resolve increasingly finer scales, and hence include increasing levels of detail. We will eventually apply the multiscale decomposition algorithm to the problem of image registration in the presence of noise, and will demonstrate the accuracy of the multiscale registration technique for noisy images such as those considered in Section 3.

We will use the following mathematical spaces in the decomposition algorithm. The space of functions of bounded variation, BV, is defined by:

$$BV = \left\{ f \quad \middle| \quad ||f||_{BV} := \sup_{h \neq 0} |h|^{-1} ||f(\cdot + h) - f(\cdot)||_{L^1} < \infty \right\}.$$

We will also use the Sobolev space $W^{-1,\infty}$ with norm given by:

$$||f||_{W^{-1,\infty}} := \sup_{g} \left[\int \frac{f(x)g(x)}{||g||_{W^{1,1}}} \, dx \right],$$

where $||g||_{W^{1,1}} := ||\nabla g||_{L^1}$.

Define the J-functional $J(f, \lambda)$ as follows:

$$J(f, \lambda) := \inf_{u+v=f} \lambda ||v||_{L^2}^2 + ||u||_{BV}, \tag{4}$$

where $\lambda > 0$ is a scaling parameter that separates the L^2 and BV terms. This functional $J(f, \lambda)$ was introduced in the context of image processing by Rudin, Osher, and Fatemi [16]. Let $[u_\lambda, v_\lambda]$ denote the minimizer of $J(f, \lambda)$. The BV component, u_λ, captures the coarse features of the image f, while the L^2 component, v_λ, captures the finer features of f such as noise. This model denoises images while preserving edges, though it requires prior knowledge on the noise scaling λ.

Tadmor, *et al.* proposed in [18] an alternative point of view in which the minimization of $J(f, \lambda)$ is interpreted as a decomposition $f = u_\lambda + v_\lambda$, where u_λ extracts the edges of f and v_λ extracts the textures of f. This interpretation depends on the scale λ, since texture at scale λ consists of edges when viewed under a refined scale. We refer to $v_\lambda = f - u_\lambda$ as the residual of the decomposition. Upon decomposing $f = u_\lambda + v_\lambda$, we proceed to decompose v_λ as follows:

$$v_\lambda = u_{2\lambda} + v_{2\lambda},$$

where

$$[u_{2\lambda}, v_{2\lambda}] = \operatorname*{arginf}_{u+v=v_\lambda} J(v_\lambda, 2\lambda).$$

Thus we obtain a two-scale representation of f given by $f \cong u_\lambda + u_{2\lambda}$, where now $v_{2\lambda} = f - (u_\lambda + u_{2\lambda})$ is the residual. Repeating this process results in the following hierarchical multiscale decomposition of f. Starting with an initial scale $\lambda = \lambda_0$, we obtain an initial decomposition of the image f:

$$f = u_0 + v_0, \quad [u_0, v_0] = \underset{u+v=f}{\operatorname{arginf}} J(f, \lambda_0).$$

We then refine this decomposition to obtain

$$v_j = u_{j+1} + v_{j+1}, \quad [u_{j+1}, v_{j+1}] = \underset{u+v=v_j}{\operatorname{arginf}} J(v_j, \lambda_0 2^{j+1}), \quad j = 0, 1, \ldots$$

After k steps of this process, we have:

$$f = u_0 + v_0 = u_0 + u_1 + v_1 = u_0 + u_1 + u_2 + v_2 = \ldots = u_0 + u_1 + \ldots + u_k + v_k, \quad (5)$$

which is a multiscale image decomposition $f \sim u_0 + u_1 + \ldots + u_k$, with a residual v_k. As k increases, the u_k components resolve edges with increasing scales $\lambda_k = \lambda_0 2^k$.

4.1.1. *Implementation of the multiscale decomposition.* As described in [18], the initial scale λ_0 should capture the smallest oscillatory scale in f, given by

$$\frac{1}{2\lambda_0} \leq ||f||_{W^{-1,\infty}} \leq \frac{1}{\lambda_0}. \quad (6)$$

However, in practice, we may not be able to determine the size of $||f||_{W^{-1,\infty}}$, so we determine the initial choice of λ_0 experimentally. Following [18], for the applications presented in this paper, we will use $\lambda_0 = 0.01$ and $\lambda_j = \lambda_0 2^j$.

We follow the numerical algorithm of [18] for the construction of our hierarchical decomposition. In each step, we use finite-difference discretization of the Euler-Lagrange equations associated with the $J(v_j, \lambda_{j+1})$ to obtain the next term, u_{j+1}, in the decomposition of the image f. Because of the singularity when $|\nabla u_\lambda| = 0$, we replace $J(f, \lambda)$ by the regularized functional

$$J^\epsilon(f, \lambda) := \inf_{u+v=f} \left\{ \lambda ||v||_{L^2}^2 + \int_\Omega \sqrt{\epsilon^2 + |\nabla u|^2}\, dx\, dy \right\}, \quad (7)$$

and at each step, we find the minimizer u_λ of J^ϵ. The Euler-Lagrange equation for $J^\epsilon(f, \lambda)$ is

$$u_\lambda - \frac{1}{2\lambda} \operatorname{div} \left(\frac{\nabla u_\lambda}{\sqrt{\epsilon^2 + |\nabla u_\lambda|^2}} \right) = f \text{ in } \Omega \ ,$$

with the Neumann boundary conditions:

$$\left. \frac{\partial u_\lambda}{\partial n} \right|_{\partial\Omega} = 0, \quad (8)$$

where $\partial\Omega$ is the boundary of the domain Ω and n is the unit outward normal. We thus obtain an expansion $f \sim \sum_{j=0}^{k} u_j$, where the u_j are constructed as approximate solutions of the recursive relation given by the following elliptic PDE:

$$u_{j+1} - \frac{1}{2\lambda_{j+1}} \operatorname{div} \left(\frac{\nabla u_{j+1}}{\sqrt{\epsilon^2 + |\nabla u_{j+1}|^2}} \right) = -\frac{1}{2\lambda_j} \operatorname{div} \left(\frac{\nabla u_j}{\sqrt{\epsilon^2 + |\nabla u_j|^2}} \right). \quad (9)$$

To numerically implement the method, we cover the domain Ω with a grid ($x_i := ih, y_j := jh$), and discretize the elliptic PDE of equation (9) as follows:.

$$u_{i,j} = f_{i,j} \tag{10}$$
$$+ \frac{1}{2\lambda h^2}\left[\frac{u_{i+1,j}-u_{i,j}}{\sqrt{\epsilon^2+(D_{+x}u_{i,j})^2+(D_{0y}u_{i,j})^2}} - \frac{u_{i,j}-u_{i-1,j}}{\sqrt{\epsilon^2+(D_{-x}u_{i,j})^2+(D_{0y}u_{i-1,j})^2}}\right]$$
$$+ \frac{1}{2\lambda h^2}\left[\frac{u_{i,j+1}-u_{i,j}}{\sqrt{\epsilon^2+(D_{0x}u_{i,j})^2+(D_{+y}u_{i,j})^2}} - \frac{u_{i,j}-u_{i,j-1}}{\sqrt{\epsilon^2+(D_{0x}u_{i,j-1})^2+(D_{-y}u_{i,j})^2}}\right], \tag{11}$$

where D_+, D_-, and D_0 denote the forward, backward, and centered divided differences, respectively. To solve the discrete regularized Euler-Lagrange equations (10), we use the Gauss-Siedel iterative method to obtain:

$$u_{i,j}^{n+1} = f_{i,j} \tag{12}$$
$$+ \frac{1}{2\lambda h^2}\left[\frac{u_{i+1,j}^{n}-u_{i,j}^{n+1}}{\sqrt{\epsilon^2+(D_{+x}u_{i,j}^{n})^2+(D_{0y}u_{i,j}^{n})^2}} - \frac{u_{i,j}^{n+1}-u_{i-1,j}^{n}}{\sqrt{\epsilon^2+(D_{-x}u_{i,j}^{n})^2+(D_{0y}u_{i-1,j}^{n})^2}}\right]$$
$$+ \frac{1}{2\lambda h^2}\left[\frac{u_{i,j+1}^{n}-u_{i,j}^{n+1}}{\sqrt{\epsilon^2+(D_{0x}u_{i,j}^{n})^2+(D_{+y}u_{i,j}^{n})^2}} - \frac{u_{i,j}^{n+1}-u_{i,j-1}^{n}}{\sqrt{\epsilon^2+(D_{0x}u_{i,j-1}^{n})^2+(D_{-y}u_{i,j}^{n})^2}}\right]. \tag{13}$$

To satisfy the Neumann boundary conditions (8), we first reflect f outside Ω by adding grid lines on all sides of Ω. As the initial condition, we set $u_{i,j}^0 = f_{i,j}$. We iterate this numerical scheme for $n = 0, 1, \ldots N$ until $||u^{n_\infty} - u^{n_\infty - 1}||$ is less than some preassigned value so that $u_{i,j}^{n_\infty}$ is an accurate approximation of the fixed point steady solution u_λ.

Finally, we denote the final solution $u_\lambda := \{u_{i,j}^{n_\infty}\}_{i,j}$. To obtain the hierarchical multiscale decomposition, we reiterate this process, each time updating f and λ in the following way:

$$\begin{array}{rcl} f_{new} & \leftarrow & f_{current} - u_\lambda, \\ \lambda_{new} & \leftarrow & 2\lambda_{current}. \end{array} \tag{14}$$

That is, at each step, we apply the $J(f_{current} - u_\lambda, 2\lambda)$ minimization to the residual $f_{current} - u_\lambda$ of the previous step. Taking $\lambda_j = \lambda_0 2^j$, we obtain after k steps a hierarchical multiscale decomposition $f = u_{\lambda_0} + u_{\lambda_1} + \ldots + u_{\lambda_k} + v_{\lambda_k}$, where we write $u_{\lambda_j} = u_j$. We call the u_j, $j = 1, 2, \ldots, k$ *the components of* f, and the v_k *the residuals*. For ease of notation, given an image f, we let $C_k(f)$ denote *the* k^{th} *scale of the image* f, $k = 1, \ldots, m$:

$$C_k(f) = \sum_{i=0}^{k-1} u_k(f). \tag{15}$$

Thus $C_k(A)$ will denote the k^{th} scale of the image A, and $C_k(B)$ will denote the k^{th} scale of image B.

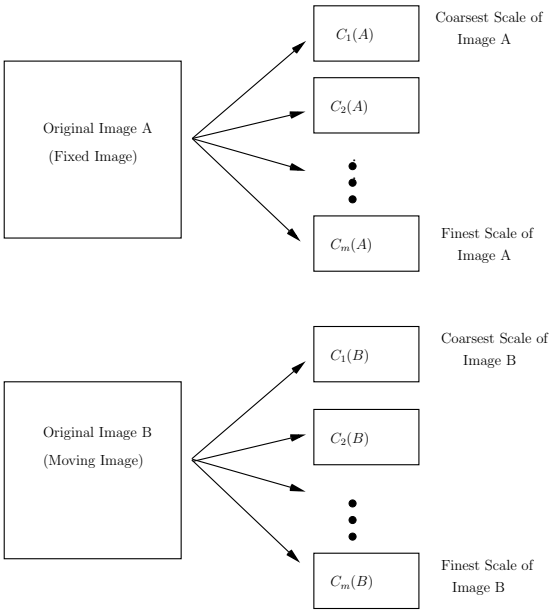

FIGURE 6. Decomposition of the fixed and moving images into a hierarchical expansion of coarse and fine scales.

4.2. **Multiscale registration algorithms.** In this section, we present two multiscale image registration algorithms that are based on the hierarchical multiscale decomposition of [18] reviewed in Section 4.1. For the general setup, consider two images A (the fixed image) and B (the moving image), and suppose that we want to register image B with image A. Suppose that one or both of the images contains a significant amount of noise. If only one of the images is noisy, we assume that it is image B. For both of the algorithms described in this section, we first apply the multiscale decomposition to both images, and let m denote the number of hierarchical steps used in the decomposition, as illustrated in Figure 6.

4.2.1. *Algorithm I: Iterated single-node multiscale registration algorithm.* In our single-node multiscale registration algorithm, Algorithm I, we iteratively register the k^{th} scale $C_k(B)$ of image B with the image A, for $k = 1, \ldots, m$. That is, we first register the first coarse scale $C_1(B)$ of the moving image with the fixed image A. The output of this registration process is the set of deformation parameters that represent the optimal deformation transformation between $C_1(B)$ and A. We then register the second scale $C_2(B)$ of the moving image with the fixed image A, *using the output deformation parameters from the first registration as the starting parameters for the second registration.* We repeat this procedure until the last scale (or desired stopping scale) is reached. That is, at each stage, we use the output deformation parameters from the previous registration as the initial parameters for the current registration. See Figure 7 for a schematic visualization of Algorithm I.

We refer to this algorithm as a *one-node multiscale registration algorithm* because we use only the multiscale components of the moving image B. Since this algorithm considers scales only of the noisy image, we expect that it will be particularly successful when only one of the images to be registered is noisy.

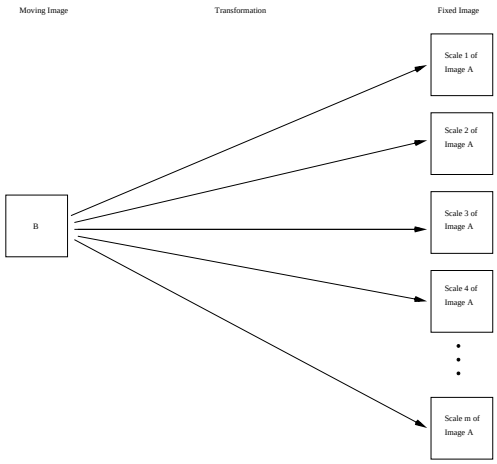

FIGURE 7. Schematic visualization of Algorithm I.

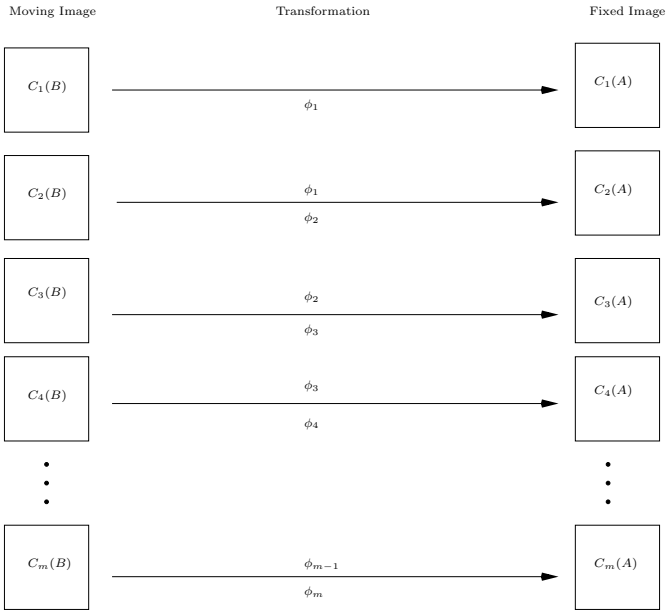

FIGURE 8. Schematic visualization of Algorithm II.

4.2.2. *Algorithm II: Iterated multinode multiscale registration algorithm.* In our multinode multiscale registration algorithm, Algorithm II, we iteratively register the k^{th} scale of image B with the k^{th} scale of image A, for $k = 1, 2, \ldots m$. See Figure 8 for a schematic visualization of Algorithm II.

We refer to this algorithm as a *multinode multiscale registration algorithm* because in each of the m registrations prescribed by the algorithm, we consider both the scales of the fixed image A and the scales of the moving image B. Since this algorithm considers scales of both the fixed and moving images, we expect that it will be particularly successful when both of the images to be registered are noisy.

TABLE 2. The correlation coefficients between the transformed moving and fixed images after each iteration of iterated single-node multiscale registration (Algorithm I). The deformed image has added noise of variance 0.6.

Iteration	1	2	3	4
ρ	0.82	0.86	0.90	0.92
Iteration	5	6	7	8
ρ	0.95	0.95	0.95	0.95

5. **Results and discussion.** In Section 3, we demonstrated that ordinary FFD registration fails to produce an acceptable result when the moving image contains a significant level of noise. In this section, we demonstrate that the multiscale methods presented in Section 4.2 enable an accurate registration of images for which ordinary deformable registration fails.

5.1. **Registration of a noisy deformed image.** Initially, we consider the case in which only one of the images to be registered (in this case, the moving image) is noisy. Consider again the original image I and the noisy deformed image $S_{0.6}$, and recall that the exact deformation transformation between the images is given by the deformation field in Figure 3.

We register the noisy deformed image $S_{0.6}$ with the original image I using Algorithm I, the iterated single-node multiscale registration algorithm. We use $m = 8$ hierarchical steps in the multiscale decomposition of the noisy deformed image $S_{0.6}$. In Table 2, we compute the correlation coefficients between the transformed moving and fixed images after iterated single-node multiscale registration, and in Figure 9, we illustrate the deformation field produced by the final iteration.

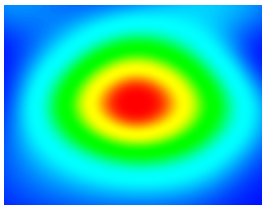

FIGURE 9. The deformation field obtained upon registering the noisy deformed image $S_{0.6}$ with the original image using the iterated single-node multiscale registration method (Algorithm I).

The results presented in Table 2 and Figure 9 demonstrate that the iterated multi-scale registration algorithm is a significant improvement over ordinary deformable registration techniques.

5.1.1. *Increasing the noise variance.* Finally, we demonstrate that the iterated single-node multiscale registration algorithm produces accurate results for noise variances δ significantly greater than those at which ordinary deformable registration fails. In Figure 10, we illustrate the noisy deformed images S_δ for very large values of the noise variance δ, and in Figure 11, we illustrate the deformation fields

TABLE 3. The correlation coefficients between the transformed moving and fixed images after iterated single-node multiscale registration (Algorithm I) for increasing values of the noise variance δ.

δ	0	0.4	0.8	1
ρ	0.96	0.95	0.95	0.95
δ	2	3	4	6
ρ	0.93	0.92	0.92	0.90

computed using the single-node iterated multiscale registration algorithm (Algorithm III) to register the noisy deformed images S_δ with the original image I for each δ illustrated in Figure 10. In Table 3, we illustrate the correlation coefficients between the images after iterated single-node multiscale registration. These results demonstrate that the iterated multiscale registration algorithm accurately registers the noisy deformed image with the original image for noise variances that are significantly greater than those at which ordinary registration fails. Recall from Section 3 that ordinary deformable registration of a noisy deformed image with a non-noisy fixed image fails for noise variances δ greater than 0.2. In Figure 11 and Table 3, we demonstrate that the iterated multiscale registration algorithm produces accurate results for noise variances δ as large as 6.

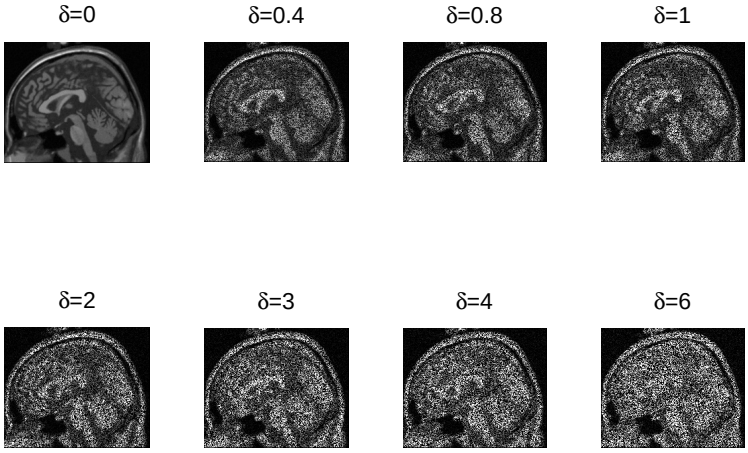

FIGURE 10. The noisy deformed images S_δ for increasing noise variances δ.

5.2. **Registration of a noisy deformed image with a noisy fixed image.** In this section, we consider the case in which both images to be registered contain significant levels of noise. We add speckle noise of variance 0.6 to the original image I, and denote this noisy image $I_{0.6}$. Our goal is to register the noisy deformed

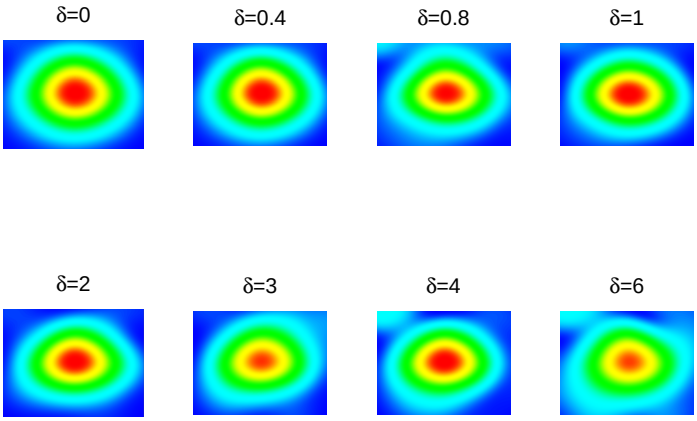

FIGURE 11. The deformation fields obtained upon registering the noisy deformed image S_δ with the original image I using Algorithm I for increasing noise variances δ.

image $S_{0.6}$ with the noisy fixed image $I_{0.6}$. In Figure 12, we illustrate both of the noisy images, as well as the deformation field produced upon registering the noisy deformed image $S_{0.6}$ with the noisy original image $I_{0.6}$ using an ordinary FFD registration technique.

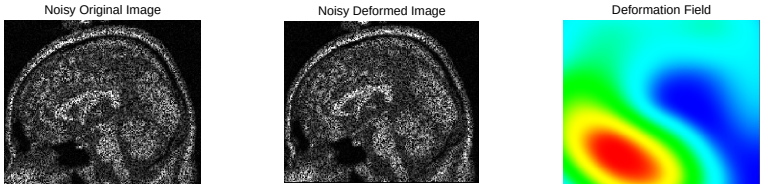

FIGURE 12. The noisy midsagittal brain slice $I_{0.6}$ (shown on the left), the noisy deformed image $S_{0.6}$ (shown in the center), and the deformation field (shown on the right) produced upon registering $S_{0.6}$ with $I_{0.6}$ using ordinary deformable registration techniques.

A visual comparison of the computed deformation field in Figure 12 with the exact deformation field in Figure 3 indicates that ordinary deformable registration of the noisy images fails. The correlation coefficient ρ between the images after ordinary deformable registration is 0.64.

5.2.1. *Multinode registration.* Since ordinary deformable registration of the noisy images fails, we register the images using our iterated multinode multiscale algorithm (Algorithm II). We use $m = 8$ hierarchical steps in the multiscale decomposition of the images. In Table 4, we compute the correlation coefficients between the

TABLE 4. The correlation coefficients between the transformed moving and fixed images after each iteration of iterated multi-node multiscale registration (Algorithm III).

Iteration	1	2	3	4
ρ	0.93	0.93	0.94	0.94
Iteration	5	6	7	8
ρ	0.94	0.95	0.95	0.95

transformed moving and fixed images after each iteration of the iterated multi-node multiscale algorithm, and in Figure 13, we illustrate the deformation field produced by the final iteration.

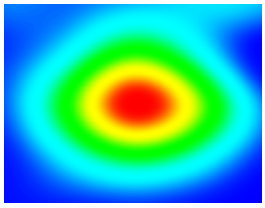

FIGURE 13. The deformation field obtained upon registering the noisy deformed image $S_{0.6}$ with the noisy original image $I_{0.6}$ using the multinode iterated multiscale registration method (Algorithm III).

The results presented in Table 4 and Figure 13 demonstrate that the iterated multiscale registration algorithm is a significant improvement over ordinary FFD registration techniques.

5.2.2. *Increasing the noise variance.* Finally, we demonstrate as in Section 5.1.1 that the iterated multinode multiscale registration algorithm produces accurate results when both of the images contain speckle noise of variance significantly greater than the level at which ordinary deformable registration fails. In Figure 15, we illustrate the deformation fields computed using the iterated multiscale registration algorithm to register the noisy deformed image S_δ with the noisy original image I_δ for increasing noise variances δ, and in Table 5, we present the correlation coefficients between the noisy images after iterated multinode multiscale registration. These results demonstrate that the iterated multiscale registration algorithm accurately registers the noisy deformed image with the noisy original image for noise variances significantly greater than those at which ordinary techniques fail; recall that ordinary deformable registration failed when *only one* of the images to be registered contain noise of variance 0.2. In Figure 14, we illustrate the noisy original and deformed images I_2 and S_2. These images contain speckle noise with variance $\delta = 2$. As demonstrated by the deformation field in Figure 15, the iterated multinode multiscale registration algorithm (Algorithm II) accurately registers these very noisy images.

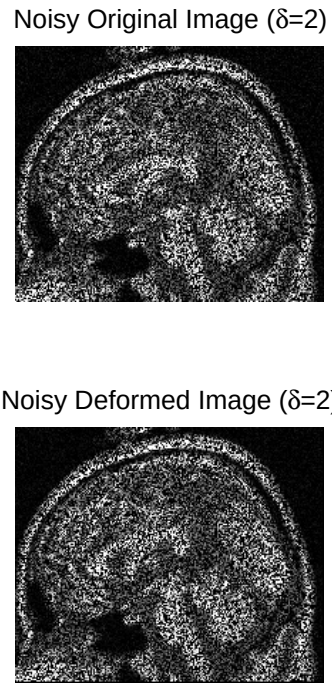

FIGURE 14. The noisy original and deformed images I_2 and S_2.

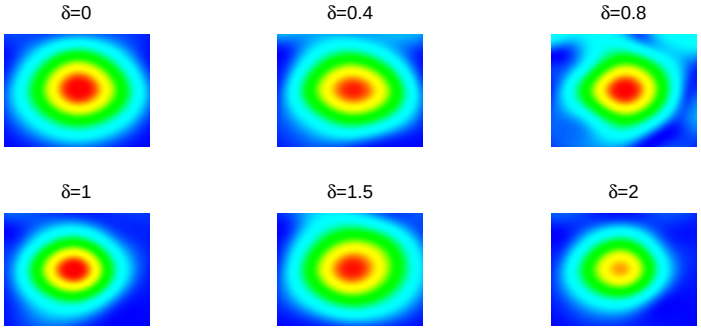

FIGURE 15. The deformation fields obtained upon registering the noisy deformed image S_δ with the noisy original image I_δ using the multi-node iterated multiscale algorithm (Algorithm II) for increasing noise variances δ.

6. **Conclusions.** While there are many existing deformable registration techniques, common approaches are shown to fail when one or more of the images to be registered contains even moderate levels of noise. We have presented deformable image registration techniques based on the hierarchical multiscale image decomposition

TABLE 5. The correlation coefficients between the transformed moving and fixed images after iterated multi-node multiscale registration (Algorithm II) for increasing values of the noise variance δ.

δ	0	0.4	0.8	1	1.5	2
ρ	0.96	0.95	0.94	0.93	0.93	0.90

of [18] that are particularly effective for registration of noisy images. This paper extends the multiscale registration techniques of [13], in which we presented algorithms for rigid image registration in the presence of noise. The multiscale decomposition of an image results in a hierarchical representation that separates the coarse and fine scales of the image. We presented two multiscale registration algorithms based on this decomposition. In the first, we follow an iterated single-node multiscale registration strategy in which we register the scales of the moving image with the fixed image, at each stage using the deformation parameters produced by the previous scale registration as the starting point for the current scale registration. In the second, we use a multi-node multiscale registration method in which we register the scales of the moving image with the scales of the fixed image, at each stage using the deformation parameters produced by the previous scale registration as the starting point for the current scale registration. Using images in which the precise deformation between the fixed and moving images is known, we have shown that the multiscale registration algorithms are indeed accurate for levels of noise much higher than the noise levels at which ordinary deformable registration techniques fail. Although we have presented our algorithm in a way that is, in principle, independent of the specific multiscale decomposition used for the expansion of the images to be registered, we have found that the hierarchical (BV, L^2) multiscale decomposition of [18] contains unique features that are not necessarily evident in other decomposition techniques. For example, information about small geometrical details is contained in both the coarse and fine scales of the image decomposition. For further details, we refer to [18]. Although the relative merits of different scale decompositions when applied to image registration is still open to debate and left for further research, we believe that the hierarchical (BV, L^2) decomposition is particularly well-suited for image registration problems. Another area for future research is combination of our multiscale registration algorithms with multi-level B-splines registration, as presented in [17]. Finally, we would like to emphasize that using the multiscale decomposition is independent of the registration method used and of the noise model. The multiscale decomposition can be used in conjunction with any registration method and can be applied to registration of images containing any type of noise, without any assumption about the particular type of noise contained in the images. In the future, we would like to work on studying convergence of registration techniques based on the hierarchical multiscale image decomposition, as well as applications of multiscale registration to other (non-medical) problems in image registration.

Acknowledgment: The work of D. Levy was supported in part by the National Science Foundation under Career Grant No. DMS-0133511. The work of L. Xing was supported in part by the Department of Defense under Grant No. PC040282 and the National Cancer Institute under Grant No. 5R01 CA98523-01.

REFERENCES

[1] A. Achim, A. Bezerianos, and P. Tsakalides, *Novel Bayesian Multiscale Method for Speckle Removal in Medical Ultrasound Images*, IEEE Trans. Med. Imaging 20 (2001), pp. 772–783.

[2] R. Bajcsy, et al., *A Computerized System for the Elastic Matching of Deformed Radiographic Images to Idealized Atlas Images*, J. Comput. Assist. Tomogr. 7 (1983), pp. 618–625.

[3] F. L. Bookstein, *Principal Warps: Thin-Plate Splines and the Decomposition of Deformations*, IEEE Trans. Pattern. Anal. 11 (1989), pp. 567–585.

[4] L. Brown, *A Survey of Image Registration Techniques*, ACM Comput. Surv. 24 (1992), pp. 325–376.

[5] G. E. Christensen, R. D. Rabbitt, and M. I. Miller, *Deformable Templates Using Large Deformation Kinematics*, IEEE Trans. Image Process. 5 (1996), pp. 1435–1447.

[6] W. R. Crum, T. Hartkens, and D. L. G. Hill, *Nonrigid Image Registration: Theory and Practice*, Brit. J. Radiol. 77 (2004), pp. 140–153.

[7] M. Ferrant, A. Navavi, B. Macq, P. M. Black, F. A. Jolesz, R. Kikinis, et al., *Serial Registration of Intraoperative MR Images of the Brain*, Med. Image Anal. 6 (2002), pp. 337–359.

[8] *Insight Segmentation and Registration Toolkit (ITK)*, http://www.itk.org.

[9] S. Lee, G. Wolberg, K.-Y. Chwa, and S. Y. Shin, *Image Metamorphosis with Scattered Feature Constraints*, IEEE Trans. Vis. Comput. Gr., 2 (1996), pp. 337–354.

[10] S. Lee, G. Wolberg, and S. Y. Shin, *Scattered Data Interpolation with Multilevel B-splines*, IEEE Trans. Vis. Comput. Gr, 3 (1997), pp. 228–244.

[11] J. Maintz and M. Viergever, A Survey of Medical Image Registration, Med. Image Anal. 2 (1998), pp. 1–36.

[12] J. Modersitzki, *Numerical Methods for Image Registration*, Oxford, 2004.

[13] D. Paquin, D. Levy, and L. Xing, *Multiscale Image Registration*, Math. Biosci. Eng. 3 (2006), pp. 389–418.

[14] V. Pekar, E. Gladilin, and K. Rohr, *An Adaptive Irregular Grid Approach for 3D Deformable Image Registration*, Phys. Med. Biol. 51 (2006), pp. 361–377.

[15] D. Roberts, A. Hartov, F. Kennedy, M. Miga, and K. Paulsen, *Intraoperative Brain Shift and Deformation: A Quantitative Analysis of Cortical Displacement in 28 Cases*, Neurosurgery 43 (1998), pp. 749–760.

[16] L. Rudin, S. Osher, and E. Fatemi, *Nonlinear Total Variation Based Noise Removal Algorithms*, Phys. D 60 (1992), pp. 259–268.

[17] D. Rueckert, L. Sonoda, C. Hayes, D. Hill, M. Leach, and D. Hawkes, *Nonrigid Registration Using Free Form Deformations: Application to Breast MR Images*, IEEE Trans. Med. Imaging 18 (1999), pp. 712–721.

[18] E. Tadmor, S. Nezzar, and L. Vese, *A Multiscale Image Representation Using Hierarchical* (BV, L^2) *Decompositions*, Multiscale Model. Simul. 2 (2004), pp. 554–579.

[19] A. Tei, A. Bharatha, M. Ferrant, P. McL. Black, F. Jolesz, R. Kikinis, and S. Warfield, *Tracking Volumetric Brain Deformation During Image Guided Neurosurgery*, VISIM: Information Retrieval and Exploration in Large Medical Image Collections, Springer Verlag, 2001.

[20] A. R. Weeks, *Fundamentals of Electronic Image Processing*, SPIE Optical Engineering Press and IEEE Press, 1996.